Coherent growth and characterization of van der Waals 1T-VSe_2 layers on GaAs(111)B using molecular beam epitaxy

Tiancong Zhu,[1,*] Dante J. O'Hara,[2,3,†] Brenton A. Noesges,[1] Menglin Zhu,[4] Jacob J. Repicky,[1] Mark R. Brenner,[5,6] Leonard J. Brillson,[1,5] Jinwoo Hwang,[4] Jay A. Gupta,[1] and Roland K. Kawakami[1,2,‡]

[1]*Department of Physics, The Ohio State University, Columbus, Ohio 43210, USA*
[2]*Program in Materials Science and Engineering, University of California, Riverside, California 92521, USA*
[3]*Materials Science Division, Lawrence Livermore National Laboratory, Livermore, California 94550, USA*
[4]*Department of Materials Science and Engineering, The Ohio State University, Columbus, Ohio 43210, USA*
[5]*Department of Electrical and Computer Engineering, The Ohio State University, Columbus, Ohio 43210, USA*
[6]*Semiconductor and Epitaxy Analysis Laboratory, The Ohio State University, Columbus, Ohio 43210, USA*

(Received 7 April 2020; accepted 26 June 2020; published 17 August 2020)

We report epitaxial growth of vanadium diselenide (VSe_2) thin films in the octahedrally coordinated (1T) structure on GaAs(111)B substrates by molecular beam epitaxy. Film thickness from a single monolayer (ML) up to 30 ML is demonstrated. Structural and chemical studies using x-ray diffraction, transmission electron microscopy, scanning tunneling microscopy, and x-ray photoelectron spectroscopy indicate high-quality thin films. Further studies show that monolayer VSe_2 films on GaAs are not air stable and are susceptible to oxidation within a matter of hours, which indicates that a protective capping layer should be employed for device applications. This work demonstrates that VSe_2, a candidate van der Waals material for possible spintronic and electronic applications, can be integrated with III-V semiconductors via epitaxial growth for two- and three-dimensional hybrid devices.

DOI: 10.1103/PhysRevMaterials.4.084002

I. INTRODUCTION

The exploration of two-dimensional (2D) materials has received appreciable attention since the first isolation of monolayer graphene [1–3]. Being only a few atoms thick, the reduced dimensionality in 2D materials can strongly influence their electronic, optical, and magnetic properties compared to their bulk analogs. For example, when reduced to monolayer thickness, the electrons in graphene behave as massless Dirac fermions [2,3] while the electronic band structure in transition-metal dichalcogenides (e.g. MoS_2, WSe_2) undergoes an indirect to direct gap transition with 100% valley selection with circular polarized light [4–9]. Other examples include the predicted tunable magnetism in hole-doped monolayer GaSe [10], strong Ising pairing in superconducting $NbSe_2$ atomic layers [11], and quantum spin Hall states in monolayer 1T′-WTe_2 [12,13]. Controlling the material thickness and further studying how their properties depend on the number of layers is essential for understanding 2D materials.

Among the family of 2D materials, VSe_2 is of particular interest, because both its electronic and magnetic properties are significantly different for the bulk and in the monolayer limit [14,15]. Bulk VSe_2 may exhibit two polymorphs, which are the semiconducting 2H (trigonal prismatic) or metallic 1T (octahedral) phase. 1T-VSe_2 forms in a layered van der Waals structure, with each V atom octahedrally coordinated by six surrounding Se atoms. Bulk 1T-VSe_2 undergoes a $(4 \times 4 \times 3)$ charge density wave (CDW) transition with $T_c = 110$ K [16–20]. However, the monolayer shows a $(\sqrt{7} \times \sqrt{3})$ CDW with altered-symmetry type compared to the (4×4) CDW in the layers of the bulk [21–24]. On the other hand, although bulk 1T-VSe_2 is reported to be paramagnetic [25,26], it has been shown to be ferromagnetic in its monolayer form with a Curie temperature above room temperature [21,24]. The drastic differences in bulk and monolayer 1T-VSe_2 make it an interesting material system to investigate how its properties change with increased thickness from the monolayer limit.

In this work, we demonstrate growth of large-area, high-quality 1T-VSe_2 on GaAs(111)B, a III-V direct gap semiconductor with favorable electronic, optoelectronic, and spintronic properties. Using molecular beam epitaxy (MBE), the film thickness is precisely controlled from single monolayers (ML) up to high thickness (30 ML). A combination of reflection high-energy electron diffraction (RHEED), x-ray diffractometry (XRD), and scanning transmission electron microscopy (STEM) confirms the formation of high-quality, rotationally oriented 1T-VSe_2 layers. X-ray photoelectron spectroscopy (XPS) measurements are conducted to confirm the chemical composition and to investigate the air stability of VSe_2 on GaAs. Furthermore, using scanning tunneling microscopy (STM), we confirm the atomic-scale structure of 1T-VSe_2 on GaAs(111)B and STM spectroscopy confirms the metallic nature of the monolayer film. These results establish

*Present address: University of California, 94720 Berkeley, CA, USA.
†Present address: Naval Research Laboratory, Washington, DC 20375, USA.
‡Corresponding author: Department of Physics, The Ohio State University, 191 W. Woodruff Ave., Columbus, OH 43210, USA; kawakami.15@osu.edu

a baseline for developing high-quality thin films of van der Waals VSe_2 on III-V semiconductors, opening the door to novel electronic and spintronic devices based on 2D and three-dimensional (3D) hybrid structures.

II. EXPERIMENTAL DETAILS

Vanadium diselenide growths are performed with van der Waals epitaxy in a Veeco GEN930 chamber with a base pressure of 2×10^{-10} Torr. Undoped GaAs(111)B substrates [AXT, single-side polished, 0.5 mm thick, $\pm$ 0.5° miscut, $1.4 \times 10^8 \Omega$ cm. "B" indicates the arsenic-terminated face of the GaAs(111) substrate] are mounted by indium bonding to a 3-in. unpolished Si wafer; then they are loaded into the chamber and annealed at 400 °C for 15 min under ultrahigh-vacuum (UHV) conditions (1×10^{-9} Torr) to remove water and gas adsorbates. The GaAs is then loaded into the growth chamber and exposed to a Ga flux (United Mineral and Chemical Corporation, 99.999 99%, 1×10^{-8} Torr) at 530 °C for 2–4 min to remove the native oxides on the surface via Ga polishing [27,28]. The substrate is then annealed at 600 °C under a Se flux (1×10^{-7} Torr) for 15 min to remove any excess oxide and terminate the surface with Se atoms; then it is cooled to the growth temperature. Elemental Se (United Mineral and Chemical Corporation, 99.9999%) is evaporated from a standard Knudsen-type effusion cell with a typical cell temperature of 170 °C and elemental V (ESPI Metals, 99.98%) is evaporated using a quad-rod electron-beam evaporator (Mantis). The beam fluxes are measured using a nude ion gauge with a tungsten filament positioned at the sample growth position and the corresponding growth rate is calibrated based on nominal film thicknesses measured by *ex situ* x-ray reflectometry (XRR, Bruker D8 Discover). The growth rate calibration is further confirmed by STM measurements of submonolayer VSe_2 grown on highly oriented pyrolytic graphite (Supplemental Material (SM), Sec. 1 [29]). *In situ* RHEED is used to monitor the growth and annealing procedures in real time with an operation voltage of 15 kV. The VSe_2 growth is performed in an adsorption-limited growth regime at a fixed beam-equivalent pressure (BEP) Se:V ratio of ∼50, where the excess Se reevaporates. For *ex situ* characterization by XRD and STEM, samples are capped with amorphous Se or Te at room temperature to protect the surface from oxidation. For *in situ* characterization by XPS and STM, we mount the GaAs substrate onto an Omicron flag-style sample holder which is loaded into a Veeco UNI-Block adapter for MBE growth. After deposition, the sample on a flag-style holder is transferred to the separate XPS or STM chamber without air exposure via a UHV suitcase. Due to the different sample mounting and its impact on growth temperature calibration, we rely on the RHEED patterns and their evolution during VSe_2 deposition to ensure that the growth occurs within the optimal temperature window.

XRD measurements are performed in a Bruker, D8 Discover system equipped with a Cu $K\alpha$ 1.54-Å wavelength x-ray source. STEM is performed using a Thermo Fisher Titan STEM operated at 300 kV. Cross-sectional TEM specimens of VSe_2 were made using a focused Ga ion beam (Thermo Fisher Helios); they are subsequently cleaned using a low-energy Ar ion mill (Fishcione NanoMill) with a minimum beam energy of 500 eV. Atomic resolution high-angle annular dark field (HAADF) images are acquired at the scattering range between 80 and 300 mrad, where the scattering intensity mostly depends on the atomic number of the elements.

XPS measurements are performed using a PHI VersaProbe 5000^{TM} system equipped with a scanning XPS microprobe x-ray source ($h\upsilon_{AlK\alpha} = 1486.6$ eV; FWHM $\leqslant$ 0.5 eV), and hemispherical energy analyzer with a pass energy of 23.5 eV and a 0.05-eV step. To minimize the effects of charging, the XPS system is equipped with a two-stage sample surface neutralization system consisting of a 10-eV electron flood gun accompanied by a 10-eV Ar^+ ion beam. Photoelectrons are collected at a takeoff angle of 45°. Curve fitting is performed using asymmetric Gaussian for metallic and selenide-bonded vanadium core levels and Voigt line shapes of oxidized vanadium.

STM measurements are performed with a CreaTec LT-STM/AFM system operating at 4.3 K in UHV with etched PtIr tips that are calibrated on clean Au(111) surfaces. We utilize conductive GaAs substrates [Si-doped GaAs(111)B from AXT, single-side polished, 0.5 mm thick, $\pm$ 0.5° miscut, $(0.8-4) \times 10^{18}$ cm^{-3} carrier concentration] to allow conduction of the tip current. Following STM measurements, image analysis is performed with WSXM software [30].

III. RESULTS AND DISCUSSION

We begin by determining the growth temperature window of VSe_2 on GaAs(111)B substrates for the highest-quality thin films. GaAs(111)B is a substrate of choice for van der Waals epitaxy [31,32] due to the hexagonal symmetry of its surface layer and the widely known passivation with Se atoms to form a GaSe-like surface. The deposition of VSe_2 on GaAs(111)B is illustrated in Fig. 1 which shows RHEED patterns as a function of thickness and growth temperature. Optimal growth conditions are found at a substrate temperature of 170 °C, Se:V flux ratio of ∼50, and a growth of 1 ML in approximately 5 min. Figures 1(a)–1(d) show the RHEED patterns for the passivated GaAs substrate and for 1-, 4-, and 10-ML VSe_2, respectively. The RHEED pattern of the VSe_2 remains streaky until approximately 30 ML (∼18.3 nm). Low-temperature growths below 150 °C result in a diffuse and dim RHEED pattern indicating an amorphous film from the large sticking coefficient and low atom mobility of Se. Figures 1(e) and 1(f) depict VSe_2 growth at temperatures higher than 200 °C (the presented data are for 350 °C), where the RHEED pattern is streaky initially but then quickly becomes spotty and modulates with azimuthal rotation after 1–2 monolayers (ML) of deposition due to three-dimensional growth. Although the growth temperature window is narrow, the RHEED patterns for 170 °C growth [Figs. 1(b)–1(d)] remain streaky and the intensity remains constant through larger thicknesses consistent with atomically smooth films. It is possible that increasing the Se flux can widen the temperature window to higher temperatures, but according to previous reports of VSe_2 grown on highly oriented pyrolytic graphite (HOPG) surfaces, a decrease in growth rate (higher chalcogen to metal flux) with a higher adatom mobility (increase in substrate temperature) can lead to large triangular islands without large-area homogenous coalescence across the whole substrate surface.

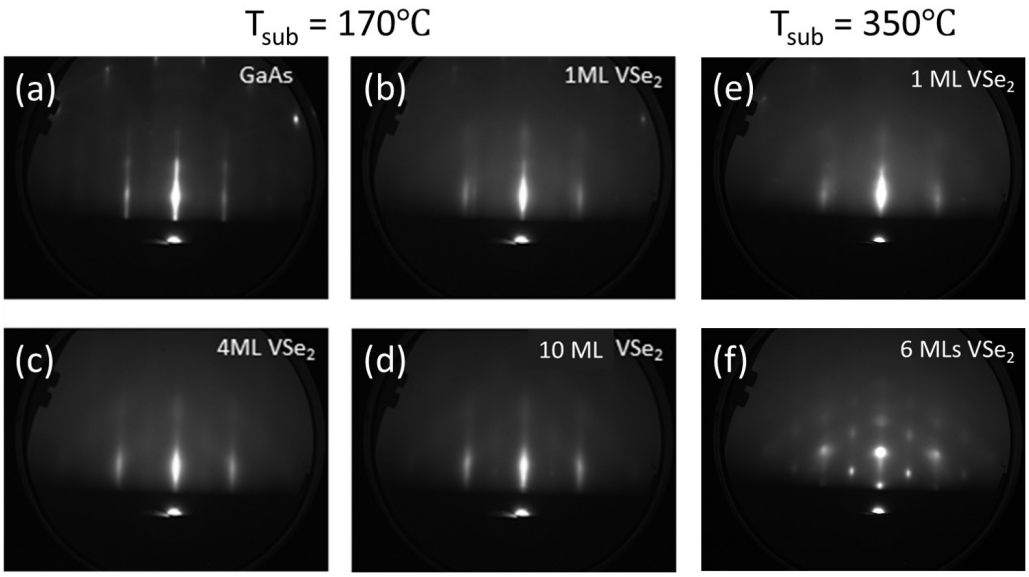

FIG. 1. RHEED patterns of VSe_2 grown on GaAs(111) viewed along the $[11\bar{2}]$ of the substrate. (a–d) Streaky RHEED patterns of GaAs substrate, 1, 4, and 10 ML of VSe_2 grown showing clear transition and streaky patterns confirming smooth and homogenous growth up to high thicknesses at a substrate temperature of 170 °C. (e,f) Elevated substrate temperature growth of VSe_2 on GaAs showing clear three-dimensional growth at 6 ML of deposition confirming a narrow temperature window.

To date, it is unclear if different island morphologies form when VSe_2 is deposited on GaAs. After deposition of 1 ML [Fig. 1(b)], the VSe_2 RHEED streaks coexist with the underlying GaAs(111). The inverse ratio of the RHEED spacing between the VSe_2 and GaAs(111) is measured to be 1.17, which is in agreement with the expected value of 1.19 for bulk in-plane lattice parameters of 1T-VSe_2(0001) ($a = 3.356$Å) and GaAs(111) ($a = 3.998$ Å) despite the nearly 19% lattice mismatch. After ∼2 ML of growth, the RHEED streaks from the underlying GaAs disappear and the VSe_2 pattern remains streaky with sixfold rotational symmetry suggesting epitaxial alignment between the two materials, $[10\bar{1}0]_{VSe_2} \| [11\bar{2}]_{GaAs}$ and $[11\bar{2}0]_{VSe_2} \| [1\bar{1}0]_{GaAs}$. The spacing of the VSe_2 streaks exhibits negligible variation with thickness, which indicates that the VSe_2 grows fully relaxed on the GaAs surface. However, RHEED patterns alone cannot distinguish whether the initial layers have true layer-by-layer growth or few-layer island formation with exposed substrate. Unfortunately, atomic force microscopy and plan-view STEM are not feasible due to the air sensitivity of the samples (discussed later). Attempts to utilize STM for large-area imaging was inconclusive due to poorer RHEED patterns resulting from growth on Si-doped GaAs substrates, which are required for the tunneling measurements (SM, Sec. 2 [29]).

We utilize x-ray diffraction (XRD) and cross-sectional STEM for detailed characterization of the interfacial and bulk structure, which is made possible by the ability to grow thick VSe_2 films. To determine the crystallographic orientation of the film, XRD measurements are performed on 30-ML VSe_2 films grown on GaAs [Fig. 2(a)]. θ-2θ XRD scans show a weak (002) 1T-VSe_2 peak at 29.3° indicating a c-axis orientation of the film and a corresponding interplanar spacing of 6.1 Å in agreement with bulk crystals [26,33,34]. To further confirm the high crystalline quality of the film, atomic structure, and interface quality, we perform cross-sectional high-resolution STEM (see Experimental Details). The high-angle annular dark field (HAADF) imaging in Fig. 2(b) shows clear van der Waals stacking from the abrupt interface between the grown VSe_2 film and the underlying GaAs substrate, which confirms a high-quality 1T structure with an epitaxial relationship of $[0002]_{VSe_2} \| [111]_{GaAs}$, and continuous growth of VSe_2 beyond 1 ML without any visible misfit dislocations propagating through the film or rotational disorder from different polytype phases (e.g., as observed in GaSe films [35]).

Air stability in ambient conditions is desirable for monolayer 2D materials. In order to study the air stability and chemical composition of our samples, we perform XPS measurements on monolayer VSe_2. Samples are first transferred from the MBE chamber to the XPS system by using a UHV suitcase. This allows us to measure the XPS spectrum of VSe_2 without any exposure to ambient conditions, which sets the baseline for the subsequent oxidation study. Figure 3 shows the XPS spectra around the V $2p$ region for as-grown monolayer VSe_2 and after 30 min or 15 h (total time) of air exposure. The spectrum for the as-grown monolayer agrees well with previous studies of thin films and bulk crystals of VSe_2 [36,37]. Distinct from studies of monolayer VSe_2 grown on HOPG where no surface oxidation was reported [36], we observe the emergence of an oxygen (O) 1s peak. The primary component of this O 1s feature is centered at 530.4 eV, indicative of metal oxide formation [38]. In addition, the characteristic vanadium peaks show clear differences after air exposure [Figs. 3(c) and 3(d)] with the V $2p_{1/2}$ and V $2p_{3/2}$ peaks shifting and splitting as a function of exposure time. After 30 min, both the V $2p_{1/2}$ and V $2p_{3/2}$ peaks lower in intensity while broadening and splitting into two peaks, indicating the as-grown V-Se bonds are being

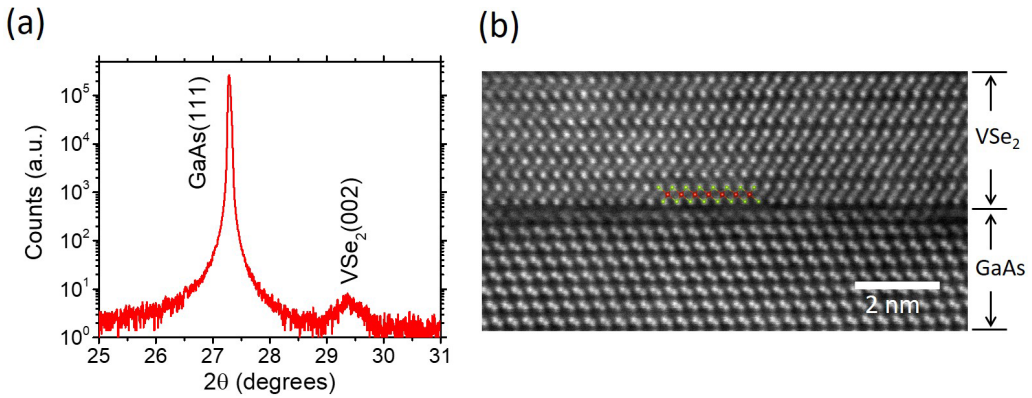

FIG. 2. Structural characterization of thick VSe_2 films on GaAs(111) substrates with (a) showing XRD reflection of (00l) planes of 1T-VSe_2 orienting on GaAs(111) surfaces and (b) STEM image (viewed along ⟨110⟩ of GaAs) showing high-quality VSe_2 layers grown on GaAs without the formation of misfit dislocations at the interface. Ball-and-stick model of 1T-VSe_2 is overlaid on the first atomic layer grown in the STEM image with red and green balls representing the V and Se atoms, respectively.

replaced by a second bond type. The identified peaks at 524.1 and 516.7 eV are indicative of a vanadium oxide structure forming at the surface. After 15 h of air exposure, the V-Se characteristic peaks at lower binding energy vanish while the vanadium oxide peaks increase in intensity with centers at 523.5 and 516.3 eV. These two distinct peaks shifted to higher binding energy after prolonged air exposure compared to the as-grown peaks are consistent with the V-Se bonds being replaced by V-O bonds, where the 14.1-eV separation of O 1*s* (530.4 eV) and V $2p_{3/2}$ (516.3 eV) after 15 h of air exposure is in rough agreement with VO_2 [39]. Similar shifts have been observed experimentally and analyzed theoretically for the oxidation of phosphorene [40]. These measurements provide evidence that monolayer VSe_2 is not oxidation resistant when grown on GaAs surfaces, in contrast to previous reports of air stability for MBE-grown monolayer VSe_2 on HOPG [36].

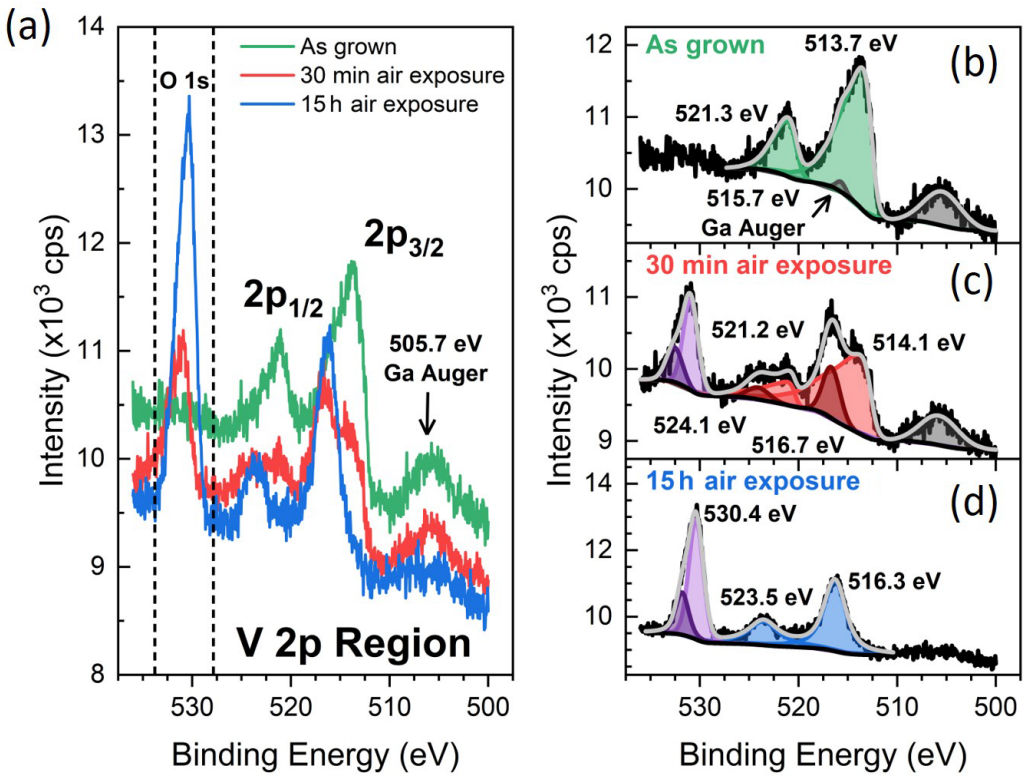

FIG. 3. Air stability of monolayer VSe_2 on GaAs. (a) Overlaid XPS measurements of the V 2*p* characteristic region before (green) and after exposure to air (red and blue) showing changes in the characteristic peaks as a function of air exposure indicative of vanadium oxidation. (b–d) V 2*p* spectra separated as individual scans and deconvolved to evaluate the peak shift for V $2p_{1/2}$ and V $2p_{3/2}$ after air exposure using asymmetric and Voigt fittings for selenide and oxide states, respectively. Air exposures of 30 min and 15 h show an evolution to a fully oxidized surface and confirm the air instability of VSe_2 grown on GaAs.

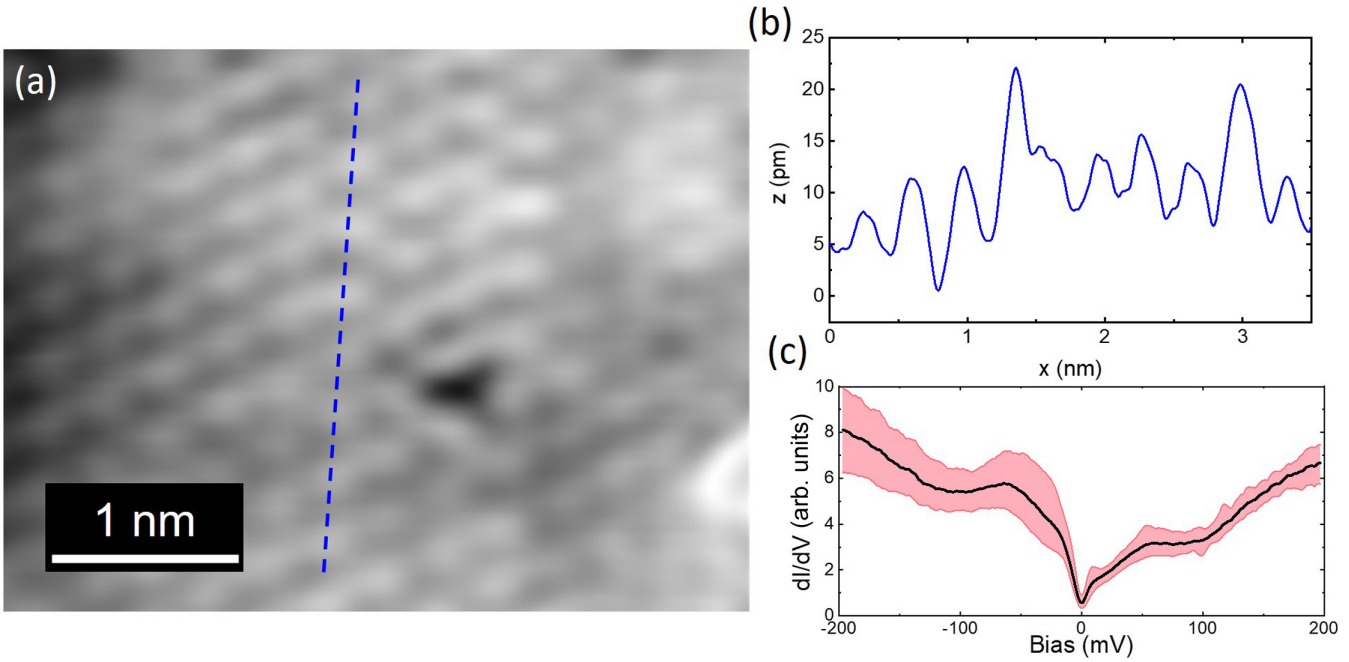

FIG. 4. STM imaging and local electronic structure of 1-ML VSe_2 with (a) showing high-resolution hexagonal lattice of VSe_2 and (b) line profile of the atomic structure along the blue dashed line in (a). (c) *dI/dV* measurement confirming the local electronic structure is metallic. The STS is performed with tip at $V_{\text{Bias}} = -200\,\text{mV}$, $I_t = 3.5\,\text{nA}$, $V_{\text{ac}} = 1\,\text{mV}$, and $f = 961\,\text{Hz}$.

However, other factors such as grain size, morphology, and stoichiometry could also affect the result and further studies are required to understand the oxidation process. These results indicate that protective capping layers should be utilized for device applications.

The formation of 1T-VSe_2 is further confirmed by low-temperature STM. As mentioned earlier, the use of heavily doped substrates for the STM study leads to more diffuse RHEED patterns (SM, Sec. 2 [29]). Nevertheless the topography measurement of a 1-ML sample [Fig. 4(a)] reveals a well-ordered hexagonal atomic structure. From this, we can obtain an in-plane lattice constant of 3.44 ± 0.10 Å, close to previous reports of 3.356 Å for bulk VSe_2 [26,41,42]. Figure 4(b) is a representative line profile showing the atomic corrugation. To investigate the local electronic structure of the VSe_2, we carry out STS measurements at low temperatures. The corresponding dI/dV spectrum is shown in Fig. 4(c), revealing the local density of states of the sample. The black curve represents the average *dI/dV* spectrum over several scans and the shaded red region represents the variation between different point spectra. The most notable feature of the *dI/dV* spectrum is the narrow dip at 0 mV with a minimum value near zero. A similar zero-bias anomaly has been observed in previous STM studies of monolayer VSe_2/HOPG at 150 K [21]. In that study, cooling from 150 K (no CDW) to 15 K induced CDW order which opened a gap of ∼55 meV in the *dI/dV* spectrum. Our results on VSe_2/GaAs at 5 K are similar to VSe_2/HOPG at 150 K, where neither shows CDW order in the STM imaging at the given temperature [Fig. 4(a)] and the *dI/dV* spectra for both exhibit a narrow zero-bias anomaly [Fig. 4(c)]. The absence of CDW order at 5 K in our samples may reflect stronger interaction and/or screening due to the doped GaAs substrate.

IV. OUTLOOK

The realization of epitaxial growth of VSe_2 on a III-V semiconductor opens the door to novel 2D/3D hybrid structures for electronic, photonic, and spintronic devices. III-V semiconductors are employed in lasers, light-emitting diodes, high-speed transistors, and optospintronic devices. Since room-temperature ferromagnetism was reported for monolayer VSe_2 [21], its integration with III-V semiconductors is particularly interesting for spintronics. However, various studies report the presence or absence of ferromagnetism in VSe_2 [21,24,43–46], indicating that the origin of ferromagnetism is not well understood and suggesting a high sensitivity to sample preparation and microstructure. Our initial magnetization studies of VSe_2 on GaAs(111)B exhibit signs of room-temperature ferromagnetism (SM, Sec. 3 [29]), but further studies are needed to establish its origin. The integration of VSe_2 monolayers and thin films onto GaAs substrates enables a different approach to investigate magnetism, spin transfer, and spin dynamics in 2D/3D hybrid structures based on time-resolved Kerr rotation [47,48]. This technique utilizes a circularly polarized pump pulse to generate electron spin polarization in GaAs and a time-delayed probe pulse to measure subsequent electron spin dynamics in GaAs and magnetization dynamics of the VSe_2. This provides an additional route to understand the origin of ferromagnetism in VSe_2 and investigate dynamical processes enabling hybrid 2D/3D spintronic devices.

V. CONCLUSIONS

In summary, we have demonstrated growth of atomically smooth and continuous thin films of 1T-VSe_2 on GaAs(111)B

by MBE. Under optimal growth conditions, we can control the thickness from a single ML up to 30 ML. Structural characterization by RHEED, XRD, STEM, and STM confirm the high quality of the interface, stacking, and surface structure. XPS experiments show poor air stability after measuring the films before and after exposure to ambient conditions. Electronic properties are investigated by low-temperature STM spectroscopy on monolayer films of VSe_2 on GaAs, which exhibit a metallic phase with a zero-bias anomaly.

ACKNOWLEDGMENTS

We thank A. J. Bishop and C. H. Lee for support on the MBE growth. This work was primarily supported by the Department of Energy (DOE) Basic Energy Sciences under Grant No. DE-SC0016379. Partial support for this project was provided by AFOSR MURI 2D MAGIC (FA9550-19-1-0390). M.Z., J.H., B.A.N., and L.J.B. acknowledge support from the Center for Emergent Materials, an NSF MRSEC, under Grants No. DMR-1420451 and No. DMR-2011876. D.J.O. recognizes support from Lawrence Livermore National Laboratory (LLNL) Lawrence Graduate Scholar Program and the GEM National Consortium Ph.D. Fellowship. Portions of this work were performed under the auspices of the US Department of Energy by Lawrence Livermore National Laboratory under Contract No. DE-AC52-07NA27344. Electron microscopy was performed at the Center for Electron Microscopy and Analysis at The Ohio State University. D.J.O. was supported by NRC/NRL while finalizing the manuscript.

T.Z. and D.J.O. contributed equally to this work.

[1] K. S. Novoselov, A. K. Geim, S. V. Morozov, D. Jiang, Y. Zhang, S. V. Dubonos, I. V. Grigorieva, and A. A. Firsov, Electric field effect in atomically thin carbon films, Science **306**, 666 (2004).

[2] K. S. Novoselov, A. K. Geim, S. V. Morozov, D. Jiang, M. I. Katsnelson, I. V. Grigorieva, S. V. Dubonos, and A. A. Firsov, Two-dimensional gas of massless Dirac fermions in graphene, Nature **438**, 197 (2005).

[3] Y. Zhang, Y.-W. Tan, H. L. Stormer, and P. Kim, Experimental observation of the quantum Hall effect and Berry's phase in graphene, Nature **438**, 201 (2005).

[4] K. F. Mak, C. Lee, J. Hone, J. Shan, and T. F. Heinz, Atomically Thin MoS_2: A New Direct-Gap Semiconductor, Phys. Rev. Lett. **105**, 136805 (2010).

[5] A. Splendiani, L. Sun, Y. Zhang, T. Li, J. Kim, C.-Y. Chim, G. Galli, and F. Wang, Emerging photoluminescence in monolayer MoS_2, Nano Lett. **10**, 1271 (2010).

[6] K. F. Mak, K. He, J. Shan, and T. F. Heinz, Control of valley polarization in monolayer MoS_2 by optical helicity, Nat. Nanotechnol. **7**, 494 (2012).

[7] H. Zeng, J. Dai, W. Yao, D. Xiao, and X. Cui, Valley polarization in MoS_2 monolayers by optical pumping, Nat. Nanotechnol. **7**, 490 (2012).

[8] T. Cao, G. Wang, W. Han, H. Ye, C. Zhu, J. Shi, Q. Niu, P. Tan, E. Wang, B. Liu, and J. Feng, Valley-selective circular dichroism of monolayer molybdenum disulphide, Nat. Commun. **3**, 887 (2012).

[9] D. Xiao, G.-B. Liu, W. Feng, X. Xu, and W. Yao, Coupled Spin and Valley Physics in Monolayers of MoS_2 and Other Group-VI Dichalcogenides, Phys. Rev. Lett. **108**, 196802 (2012).

[10] T. Cao, Z. Li, and S. G. Louie, Tunable Magnetism and Half-Metallicity in Hole-Doped Monolayer GaSe, Phys. Rev. Lett. **114**, 236602 (2015).

[11] X. Xi, Z. Wang, W. Zhao, J.-H. Park, K. T. Law, H. Berger, L. Forró, J. Shan, and K. F. Mak, Ising pairing in superconducting $NbSe_2$ atomic layers, Nat. Phys. **12**, 139 (2016).

[12] Z. Fei, T. Palomaki, S. Wu, W. Zhao, X. Cai, B. Sun, P. Nguyen, J. Finney, X. Xu, and D. H. Cobden, Edge conduction in monolayer WTe_2, Nat. Phys. **13**, 677 (2017).

[13] S. Tang, C. Zhang, D. Wong, Z. Pedramrazi, H.-Z. Tsai, C. Jia, B. Moritz, M. Claassen, H. Ryu, S. Kahn, J. Jiang, H. Yan, M. Hashimoto, D. Lu, R. G. Moore, C.-C. Hwang, C. Hwang, Z. Hussain, Y. Chen, M. M. Ugeda *et al.*, Quantum spin Hall state in monolayer 1T′-WTe_2, Nat. Phys. **13**, 683 (2017).

[14] Y. Ma, Y. Dai, M. Guo, C. Niu, Y. Zhu, and B. Huang, Evidence of the existence of magnetism in pristine VX_2 monolayers (X = S, Se) and their strain-induced tunable magnetic properties, ACS Nano **6**, 1695 (2012).

[15] W. Zhang, L. Zhang, P. K. J. Wong, J. Yuan, G. Vinai, P. Torelli, G. van der Laan, Y. P. Feng, and A. T. S. Wee, Magnetic transition in monolayer VSe_2 via interface hybridization, ACS Nano **13**, 8997 (2019).

[16] Á. Pásztor, A. Scarfato, C. Barreteau, E. Giannini, and C. Renner, Dimensional crossover of the charge density wave transition in thin exfoliated VSe_2, 2D Mater. **4**, 041005 (2017).

[17] V. N. Strocov, M. Shi, M. Kobayashi, C. Monney, X. Wang, J. Krempasky, T. Schmitt, L. Patthey, H. Berger, and P. Blaha, Three-Dimensional Electron Realm in VSe_2 by Soft-X-Ray Photoelectron Spectroscopy: Origin of Charge-Density Waves, Phys. Rev. Lett. **109**, 086401 (2012).

[18] K. Tsutsumi, X-ray-diffraction study of the periodic lattice distortion associated with a charge-density wave in 1T-VSe_2, Phys. Rev. B **26**, 5756 (1982).

[19] D. J. Eaglesham, R. L. Withers, and D. M. Bird, Charge-density-wave transitions in 1T-VSe_2, J. Phys. C: Solid State Phys. **19**, 359 (1986).

[20] A. M. Woolley and G. Wexler, Band structures and Fermi surfaces for 1T-TaS_2, 1T-$TaSe_2$ and 1T-VSe_2, J. Phys. C: Solid State Phys. **10**, 2601 (1977).

[21] M. Bonilla, S. Kolekar, Y. Ma, H. C. Diaz, V. Kalappattil, R. Das, T. Eggers, H. R. Gutierrez, M.-H. Phan, and M. Batzill, Strong room-temperature ferromagnetism in VSe_2 monolayers on van der Waals substrates, Nat. Nanotechnol. **13**, 289 (2018).

[22] P. Chen, W. W. Pai, Y.-H. Chan, V. Madhavan, M. Y. Chou, S.-K. Mo, A.-V. Fedorov, and T.-C. Chiang, Unique Gap Structure and Symmetry of the Charge Density Wave in Single-Layer VSe_2, Phys. Rev. Lett. **121**, 196402 (2018).

[23] G. Duvjir, B. K. Choi, I. Jang, S. Ulstrup, S. Kang, T. Thi Ly, S. Kim, Y. H. Choi, C. Jozwiak, A. Bostwick, E. Rotenberg, J.-G. Park, R. Sankar, K.-S. Kim, J. Kim, and Y. J. Chang, Emergence of a metal-insulator transition and high-temperature charge-density waves in VSe_2 at the monolayer limit, Nano Lett. **18**, 5432 (2018).

[24] P. M. Coelho, K. Nguyen Cong, M. Bonilla, S. Kolekar, M.-H. Phan, J. Avila, M. C. Asensio, I. I. Oleynik, and M. Batzill, Charge density wave state suppresses ferromagnetic ordering in VSe_2 monolayers, J. Phys. Chem. C **123**, 14089 (2019).

[25] C. F. van Bruggen and C. Haas, Magnetic susceptibility and electrical properties of VSe_2 single crystals, Solid State Commun. **20**, 251 (1976).

[26] M. Bayard and M. J. Sienko, Anomalous electrical and magnetic properties of vanadium diselenide, J. Solid State Chem. **19**, 325 (1976).

[27] J. H. Lee, Zh. M. Wang, and G. J. Salamo, Ga-triggered oxide desorption from GaAs(100) and non-(100) substrates, Appl. Phys. Lett. **88**, 252108 (2006).

[28] A. Kawaharazuka and Y. Horikoshi, Behavior of Ga atoms deposited on GaAs (111)B and (111)A surfaces, J. Cryst. Growth **477**, 25 (2017).

[29] See Supplemental Material at http://link.aps.org/supplemental/10.1103/PhysRevMaterials.4.084002 for additional STM, RHEED, and SQUID data.

[30] I. Horcas, R. Fernández, J. M. Gómez-Rodríguez, J. Colchero, J. Gómez-Herrero, and A. M. Baro, WSXM: A software for scanning probe microscopy and a tool for nanotechnology, Rev. Sci. Instrum. **78**, 013705 (2007).

[31] A. Koma, Van der Waals epitaxy–a new epitaxial growth method for a highly lattice-mismatched system, Thin Solid Films **216**, 72 (1992).

[32] L. A. Walsh and C. L. Hinkle, Van der Waals epitaxy: 2D materials and topological insulators, Appl. Mater. Today **9**, 504 (2017).

[33] A. H. Thompson and B. G. Silbernagel, Correlated magnetic and transport properties in the charge-density-wave states of VSe_2, Phys. Rev. B **19**, 3420 (1979).

[34] L. F. Schneemeyer, A. Stacy, and M. J. Sienko, Effect of nonstoichiometry on the periodic lattice distortion in vanadium diselenide, Inorg. Chem. **19**, 2659 (1980).

[35] C. H. Lee, S. Krishnamoorthy, D. J. O'Hara, M. R. Brenner, J. M. Johnson, J. S. Jamison, R. C. Myers, R. K. Kawakami, J. Hwang, and S. Rajan, Molecular beam epitaxy of 2D-layered gallium selenide on GaN substrates, J. Appl. Phys. **121**, 094302 (2017).

[36] Z.-L. Liu, X. Wu, Y. Shao, J. Qi, Y. Cao, L. Huang, C. Liu, J.-O. Wang, Q. Zheng, Z.-L. Zhu, K. Ibrahim, Y.-L. Wang, and H.-J. Gao, Epitaxially grown monolayer VSe_2: An air-stable magnetic two-dimensional material with low work function at edges, Sci. Bull. **63**, 419 (2018).

[37] Q. Cao, F. F. Yun, L. Sang, F. Xiang, G. Liu, and X. Wang, Defect introduced paramagnetism and weak localization in two-dimensional metal VSe_2, Nanotechnology **28**, 475703 (2017).

[38] J. F. Moulder, W. F. Stickle, P. E. Sobol, K. D. Bomben, and J. Chastain, *Handbook of X-Ray Photoelectron Spectroscopy: A Reference Book of Standard Spectra for Identification of XPS Data*, (Perkin-Elmer, Waltham, MA, 1992).

[39] J. Mendialdua, R. Casanova, and Y. Barbaux, XPS studies of V_2O_5, V_6O_{13}, VO_2 and V_2O_3, J. Electron Spectrosc. Relat. Phenom. **71**, 249 (1995).

[40] T. Yang, B. Dong, J. Wang, Z. Zhang, J. Guan, K. Kuntz, S. C. Warren, and D. Tománek, Interpreting core-level spectra of oxidizing phosphorene: Theory and experiment, Phys. Rev. B **92**, 125412 (2015).

[41] D. Zhang, J. Ha, H. Baek, Y.-H. Chan, F. D. Natterer, A. F. Myers, J. D. Schumacher, W. G. Cullen, A. V. Davydov, Y. Kuk, M. Y. Chou, N. B. Zhitenev, and J. A. Stroscio, Strain engineering a $4a \times \sqrt{3}a$ charge-density-wave phase in transition-metal dichalcogenide 1T-VSe_2. Phys. Rev. Mater. **1**, 024005 (2017).

[42] B. Giambattista, C. G. Slough, W. W. McNairy, and R. V. Coleman, Scanning tunneling microscopy of atoms and charge-density waves in 1T-TaS_2,1T-TaS_2, and 1T-VSe_2, Phys. Rev. B **41**, 10082 (1990).

[43] K. Xu, P. Chen, X. Li, C. Wu, Y. Guo, J. Zhao, X. Wu, and Y. Xie, Ultrathin nanosheets of vanadium diselenide: A metallic two-dimensional material with ferromagnetic charge-density-wave behavior, Angew. Chem., Int. Ed. **52**, 10477 (2013).

[44] J. Feng, D. Biswas, A. Rajan, M. D. Watson, F. Mazzola, O. J. Clark, K. Underwood, I. Marković, M. McLaren, A. Hunter, D. M. Burn, L. B. Duffy, S. Barua, G. Balakrishnan, F. Bertran, P. Le Fèvre, T. K. Kim, G. van der Laan, T. Hesjedal, P. Wahl *et al.*, Electronic structure and enhanced charge-density wave order of monolayer VSe_2, Nano Lett. **18**, 4493 (2018).

[45] G. Chen, S. T. Howard, A. B. Maghirang III, K. N. Cong, K. Cai, S. C. Ganguli, W. Sweich, E. Morosan, I. I. Oleynik, F.-C. Chuang, H. Lin, and V. Madhavan, Correlating structural, electronic, and magnetic properties of epitaxial VSe_2 thin films, arXiv:1912.12798.

[46] S. Kezilebieke, M. N. Huda, P. Dreher, I. Manninen, Y. Zhou, J. Sainio, R. Mansell, M. M. Ugeda, S. van Dijken, H.-P. Komsa, and P. Liljeroth, Electronic and magnetic characterization of epitaxial VSe_2 monolayers on superconducting $NbSe_2$, Commun. Phys. 3, 116 (2020)..

[47] S. A. Crooker, J. J. Baumberg, F. Flack, N. Samarth, and D. D. Awschalom, Terahertz Spin Precession and Coherent Transfer of Angular Momenta in Magnetic Quantum Wells, Phys. Rev. Lett. **77**, 2814 (1996).

[48] R. K. Kawakami, Y. Kato, M. Hanson, I. Malajovich, J. M. Stephens, E. Johnston-Halperin, G. Salis, A. C. Gossard, and D. D. Awschalom, Ferromagnetic imprinting of nuclear spins in semiconductors, Science **294**, 131 (2001).